Direct observation of heat dissipation in individual suspended carbon nanotubes using a two-laser technique

I-Kai Hsu,[1] Michael T. Pettes,[2] Mehmet Aykol,[3] Chia-Chi Chang,[4] Wei-Hsuan Hung,[1] Jesse Theiss,[3] Li Shi,[2] and Stephen B. Cronin[3,a)]
[1]*Department of Materials Science, University of Southern California, Los Angeles, California 90089, USA*
[2]*Department of Mechanical Engineering and Center for Nano and Molecular Science and Technology, Texas Materials Institute, University of Texas of Austin, Austin, Texas 78712, USA*
[3]*Department of Electrical Engineering, University of Southern California, Los Angeles, California 90089, USA*
[4]*Department of Physics, University of Southern California, Los Angeles, California 90089, USA*

(Received 21 March 2011; accepted 23 July 2011; published online 31 August 2011)

A two-laser technique is used to investigate heat spreading along individual single walled carbon nanotube (SWCNT) bundles in vacuum and air environments. A 532 nm laser focused on the center of a suspended SWCNT bundle is used as a local heat source, and a 633 nm laser is used to measure the spatial temperature profile along the SWCNT bundle by monitoring the *G* band downshifts in the Raman spectra. A constant temperature gradient is observed when the SWCNT bundle is irradiated in vacuum, giving direct evidence of diffusive transport of the phonons probed by the Raman laser. In air, however, we observe an exponentially decaying temperature profile with a decay length of about 7 μm, due to heat dissipation from the SWCNT bundle to the surrounding gas molecules. The thermal conductivity of the suspended carbon nanotube (CNT) is determined from its electrical heating temperature profile as measured in vacuum and the nanotube bundle diameter measured via transmission electron microscopy. Based on the exponential decay curves measured in three different CNTs in air, the heat transfer coefficient between the SWCNTs and the surrounding air molecules is found to range from 1.5×10^3 to 7.9×10^4 W/m^2 K, which is smaller than the 1×10^5 W/m^2 K thermal boundary conductance value calculated using the kinetic theory of gases. This measurement is insensitive to the thermal contact resistance, as no temperature drops occur at the ends of the nanotube. It is also insensitive to errors in the calibration of the *G* band temperature coefficient. The optical absorption is also obtained from these results and is on the order of 10^{-5}. © *2011 American Institute of Physics*. [doi:10.1063/1.3627236]

I. INTRODUCTION

As the power densities of micro- and nano-electronic devices continue to increase, thermal management is becoming an increasingly important area of research. In coming years, device performances will rely intimately on the development of new thermal management solutions. The heat generated in micro- and nano-scale devices can be dissipated to the substrate or taken away by the surrounding gas or liquid molecules. Carbon nanotubes (CNTs) have been investigated for applications as thermal interfacial materials between hot device areas and heat sinks due to their extremely high thermal conductivity.[1] A number of studies have shown mixed results for CNT-containing thermal interface materials, for which the performance was mainly limited by the small volume fraction of CNTs in contact with both mating surfaces and the high interfacial resistances in the contact area.[2–5] However, Kordas *et al*. have shown moderate enhancements of the heat dissipation to gaseous environments on a chip embedded with vertical microfin structures made of CNTs.[6] In general, decreasing the fin diameter results in increasing the surface to volume ratio and, thus, heat dissipation to the surrounding gas molecules. If the heat transfer from the fin is based on free convection, the free convection coefficient (h) on a horizontal rod is known to increase with decreasing diameter (d) according to a power law $h \propto (k/d)R_a^n$,[7] where k is the thermal conductivity of the gas and R_a is the Rayleigh number, which is proportional to d^3. The exponent n increases from 0.058 to 0.333 when the Rayleigh number increases from 10^{-10} to 10^{12}.[7] Therefore, a rod with a diameter as small as a single-walled carbon nanotube (SWCNT) is expected to have a higher gas heat transfer coefficient as compared to fins of much larger diameters. However, the Rayleigh number associated with 1 to 10 nm diameter SWCNTs is on the order of 10^{-14} to 10^{-17}, which is much smaller than the 10^{-10} to 10^{12} range that has been studied in the past. Therefore, heat transfer from a nanotube fin needs to be described with the use of the kinetic theory of molecules instead of free convection or other continuum approximations. In order to establish how efficiently the heat can be dissipated from a hot surface when bridging the heat sink with a carbon nanotube fin, thermal transport in and thermal exchange between the surface of an isolated CNT and its surrounding gas environment must be studied.

Measuring the thermal transport and heat dissipation in individual CNTs presents several challenges, mainly because of their small size. Several different thermal measurement

a)Author to whom correspondence should be addressed. Electronic mail: scronin@usc.edu.

 © 2011 American Institute of Physics

Downloaded 26 Sep 2011 to 128.125.121.154. Redistribution subject to AIP license or copyright; see http://jap.aip.org/about/rights_and_permissions

techniques have been developed, including micro-fabricated suspended thermometers,[8–10] electronic burnout measurements,[11] the 3ω method,[12,13] and the interpretation of the current-voltage characteristics of CNT systems.[14,15] However, the measurements described above consider heat conduction only along the nanotube itself, and they do not consider the heat transfer from the nanotube to surrounding gas environments.

More recently, the spatial temperature profile, temperature drop at the contacts, and thermal contact resistance were measured on an electrically heated SWCNT using micro-Raman spectroscopy.[14] In other recent work, micro-Raman spectroscopy has been used to measure the thermal transport in suspended CNTs, where thermal equilibrium was established.[15–17] However, most of these prior Raman measurements have been conducted in air, and the heat dissipation through the air has been ignored. In one very recent measurement, the temperature distribution of electrically heated nanotubes a few microns long has been measured using Raman spectroscopy in both vacuum and different gas environments.[18] Much higher temperatures were observed in vacuum than in the various gases, which indicates that the heat dissipation to the surrounding gas medium is significant. Moreover, this work showed that polyatomic molecules remove more heat from the CNT than do monatomic molecules.[18] However, because of the potentially large electrical contact resistance in these short nanotube samples, the thermal conductivity of the nanotube and the nanotube-gas heat transfer coefficient could not be quantified accurately from the measurement results.

Although a direct measurement of the gas heat transfer coefficient of individual carbon nanotubes is still lacking, the thermal boundary conductance (TBC) between the surface of a CNT and various gas molecules has been investigated theoretically in several works. Molecular dynamics (MD) simulations have predicted the thermal boundary conductance of a single walled CNT surrounded by argon molecules as 2.4 MW/m^2 K and 1.6 MW/m^2 K in solid and liquid argon environments, respectively.[19] A larger TBC was also calculated for a CNT in a liquid octane environment.[20] Hu *et al.* simulated the TBC between a CNT and air as 0.1 MW/m^2 K at 1 atm.[21] In addition to MD simulations, the theoretical value of gas conductance per unit surface area can be estimated using a simple gas kinetic model as a function of the molecular density, the root mean square velocity of the gas molecules, and the heat capacity of the gas.[22] This yields an upper bound of the CNT/N_2 and CNT/O_2 TBCs of 0.11 MW/m^2 K and 0.1 MW/m^2 K at room temperature and 1 atm, respectively, close to Hu *et al.*'s MD result.

In the work presented here, the thermal conductivity of a suspended CNT is first measured in vacuum using the same electrical-heating method reported in our previous publications and those of others.[14,15,18] We then use one focused laser to create local heating in the suspended CNT and another laser to measure the temperature distribution along the nanotube using Raman spectroscopy. By analyzing the normalized temperature decay curves along the CNT in a gas environment, we obtain the heat transfer coefficient to the surrounding gas molecules. The measurement is insensitive to the thermal contact resistance, as no temperature drops are observed at the ends of the nanotube. Furthermore, it is also insensitive to the errors in the calibration of the *G* band temperature coefficient.

II. EXPERIMENTAL METHODS AND RESULTS

SWCNT bundles are grown via chemical vapor deposition[23] and suspended across 30 to 100 μm wide slits etched through a 380 μm thick, 3 mm × 3 mm silicon substrate. The slits are fabricated via reactive ion etching through the back of a double-sided $SiN_x/Si/SiN_x$ wafer, followed by a potassium hydroxide etch and subsequent removal of the top SiN_x layer. A SiO_2 film 400 nm in thickness is then grown on the back-etched samples in order to prevent electrical shorting by unintentionally grown CNTs connecting the side walls of the slit and the electrodes. Following the CNT growth, Ti/Pd electrodes are deposited at the two ends of the CNT using a shadow mask.

Figure 1 shows a schematic diagram of the two-laser measurement setup, in which a 532 nm laser is focused and aligned underneath the suspended CNT through an aberration corrected 40× objective lens with a numerical aperture of 0.6. This produces a 0.75 μm diameter laser spot for locally heating the CNT. Raman spectra are measured with a 633 nm laser focused through another 40× or 50× objective lens incident on the top of the CNT, as shown schematically in Fig. 1. Raman spectra are collected in a Renishaw *inVia* micro-Raman spectrometer. Spatial mapping of the Raman spectra is achieved using a PRIOR ProScan II high precision microscope stage. Also, a cylindrical lens is placed in the 633 nm laser beam path to create a line-focused laser profile. The cylindrical lens spreads the incident laser beam in the *x*-direction (along the CNT). Because the grating spreads the spectrum in the *y*-direction on the detector, simultaneous spectra can be taken by collecting the full 2D image reaching the detector array in the spectrometer. This allows more than 30 μm of spatially mapped micro-Raman spectra to be collected simultaneously. Using this technique, the resolution of each pixel is 1.25 μm and 1 μm for the 40× and 50× objective lenses, respectively. This increases the speed at which these measurements can be performed by a factor of 30, eliminating issues associated with sample drift during the measurement. The temperature-induced *G* band downshifts are calibrated in a Linkam THMSE 600 temperature controlled stage as $-0.0226\ cm^{-1}/K$, which is consistent with values presented previously in the literature.[14,16,24]

Figure 2(a) shows a scanning electron microscopy (SEM) image of a 76 μm long suspended CNT bundle. The

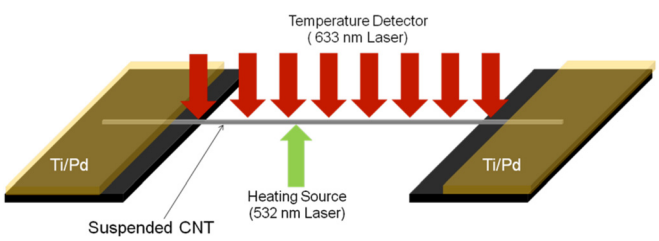

FIG. 1. (Color online) Schematic diagram of the two-laser measurement setup.

Downloaded 26 Sep 2011 to 128.125.121.154. Redistribution subject to AIP license or copyright; see http://jap.aip.org/about/rights_and_permissions

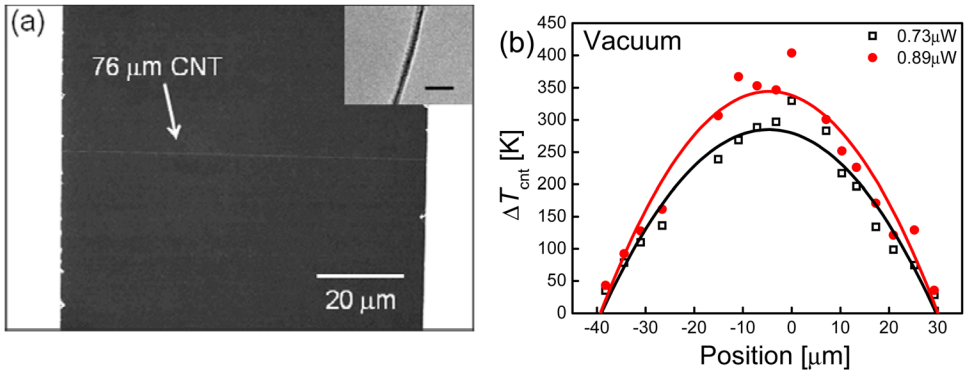

FIG. 2. (Color online) (a) SEM image of a 76 μm long suspended CNT. (b) Temperature profiles measured along the CNT in vacuum under different electrical heating powers. The TEM image of the measured CNT is shown in the inset of (a). The scale bar is 50 nm.

diameter of this bundle was determined via transmission electron microscopy (TEM) to be 12.5 nm, as shown in the inset of Fig. 2(a). The parabolic G band Raman temperature profiles along this 76 μm long CNT measured under different electrical powers are shown in Fig. 2(b). The thermal conductivity is obtained from the quadratic coefficient of the second order polynomial fit to the temperature profile obtained in vacuum, together with the measured electrical power, suspended CNT length, and diameter, as described in a previous publication.[18] Here, the thermal conductivity of the CNT bundle is determined to be 163 W/m K. The estimated heat loss due to radiation in the CNT can be expressed as $Q_{\mathrm{rad}} = \varepsilon_{\mathrm{cnt}} A_{\mathrm{cnt}} \sigma (T_{\mathrm{cnt}}{}^4 - T_{\mathrm{o}}{}^4)$, where $\varepsilon_{\mathrm{cnt}}$, σ, A_{cnt}, T_{cnt}, and T_{o} are the emissivity, Stephan-Boltzmann constant, surface area of a SWCNT bundle, average temperature of a SWCNT, and ambient temperature, respectively.[7] If the CNT is taken as a blackbody, with $\varepsilon_{\mathrm{cnt}} = 1$, the radiation heat loss for sample 1 listed in Table I can be calculated as 0.395 nW, which is about 4 orders of magnitude smaller than the total electrical heating power, 0.89 μW. We therefore can neglect the radiation heat loss in the CNT.

Figure 3(a) shows the temperature profiles of a suspended CNT sample measured using the two-laser technique. Here, the CNT was locally heated by a focused laser beam while the temperature distribution along the nanotube was measured using a second laser. The temperature profiles measured in vacuum show linear temperature profiles, and the peak temperature moves with the heating laser spot location. The linear temperature profiles are expected for a diffusive thermal conductor with a point heat source. In comparison, the temperature profile measured in air is nonlinear and decays exponentially away from the heating laser spot, as shown in Fig. 3(b). Moreover, the maximum temperature increase in the CNT is only 150 K when irradiated in air at 35 mW, as compared to 275 K when irradiated in vacuum at the same location with only 30 mW, further indicating the non-negligible heat dissipation to the surrounding gas environment.

Similar nonlinear temperature profiles were observed in other suspended CNT samples in air. Figure 4 shows the normalized temperature profile of another sample measured using the two-laser technique. Here, the location of the focused laser heating spot is defined between $x = -0.375$ and 0.375 μm. For this sample, the temperature decays rapidly with an exponential dependence over a few microns. This implies that heat dissipation from the long CNT to the surrounding air molecules plays an important role in the heat dissipation. Because the heating laser spot is defined between $x = 0.375$ and $x = -0.375$ μm, the normalized temperature profile is fit to an exponential function from $x = \pm 0.375$ μm toward both edges of the trench, as shown by the red curve in Fig. 4.

The temperature profiles measured in vacuum and in air indicate that the thermal transport is diffusive. Therefore, the spatial temperature profile measured in air can be analyzed using the heat diffusion equation, as expressed in Eq. (1):

$$\frac{d^2T}{dx^2} - \frac{gP}{kA}(T - T_o) = 0. \tag{1}$$

Here, T, T_o, P, A, k, and g represent the temperature of the CNT, the ambient temperature of the surrounding gas environment, the CNT's perimeter, the cross-sectional area, the thermal conductivity, and the heat transfer coefficient between the CNT and air, respectively. Because the nanotube temperature decays to nearly room temperature within a short distance from the laser spot, essentially all of the optical heating is dissipated to the surrounding air molecules, and we can neglect the heat lost through the ends of the CNT. In this case, the temperature profile can be considered as the following for an infinitely long fin of uniform diameter[7]:

$$\frac{\Delta T(x)}{\Delta T_{\mathrm{H}}} = e^{-mx}, \tag{2}$$

TABLE I. Summary of the sample dimensions and measurement results of three suspended CNTs.

Sample	L_{cnt} (μm)	d_{cnt} (nm)	R_{cnt} (MΩ)	k (W/m K)	m_{L}, m_{R} ($\times 10^5$ m^{-1})	g ($\times 10^4$ W/m^2 K)	α
1	76.3	12.54	0.1	163	3.93, 3.78	7.91, 7.31	2.8×10^{-5}
2	89	12.9	0.27	66	2.89, 4.13	1.79, 3.66	1.4×10^{-5}
3	31	9.89	1.25	16	4.05, 2.61	0.35, 0.15	5.9×10^{-6}

Downloaded 26 Sep 2011 to 128.125.121.154. Redistribution subject to AIP license or copyright; see http://jap.aip.org/about/rights_and_permissions

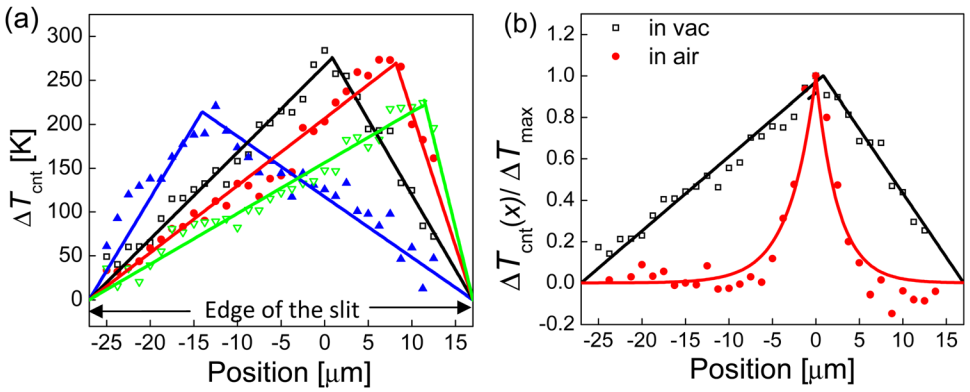

FIG. 3. (Color online) (a) Temperature profiles along a 44 μm suspended CNT measured in vacuum. Each symbol represents a different location of the 532 nm focused laser heat source. (b) Comparison of the normalized temperature profiles measured in vacuum and in air.

where ΔT_H is the highest temperature reached along the CNT, located one heating laser radius away from the center of the heating spot, and $m \equiv \sqrt{gP/kA}$. From the exponential fits shown in Fig. 4, the values of m obtained were 3.78×10^5 m^{-1} and 3.93×10^5 m^{-1} for the right and left segments of the CNT, respectively. It is worth noting that m depends on only the normalized temperature profile, making this measurement insensitive to the precise value of the temperature coefficient of the G band (-0.0226 cm^{-1}/K). Based on these values of m, we establish the ratio of the heat transfer coefficient to the thermal conductivity of the CNT (g/k) as 448 m^{-1} and 484 m^{-1}. Based on the thermal conductivities of the CNT obtained from the electrical heating data measured in vacuum (Fig. 2), we can establish the upper and lower bounds of the heat transfer coefficient as 7.9×10^4 W/m^2 K and 7.3×10^4 W/m^2 K, respectively.

The thermal decay length defines the minimum length that a CNT needs in order to exchange 99% of the heat generated by a local heat source with the surrounding gas environment, and this is given by the relation $L_{\min} = 2.65/m$ when $e^{-2.65} = 0.01$. This gives $L_{\min}$ values of 7.0 μm and 6.7 μm for the right and left segments of the CNT, respectively. The power absorbed in the CNT can also be evaluated by the temperature gradients observed in the interface between the laser spot and the left and right segments of the CNT, as given by

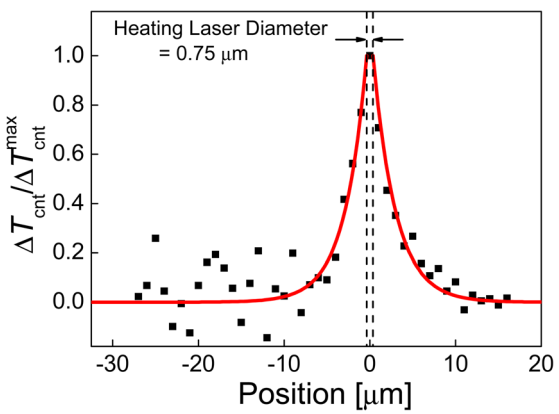

FIG. 4. (Color online) Normalized temperature profile along a suspended CNT measured using the two-laser measurement technique. The solid red curve shows the exponential fit to the normalized temperature profiles starting from $x = \pm 0.375$ μm.

$$\dot{Q} = kA \left.\frac{d\Delta T(x)}{dx}\right|_{x=-0.375\mu m} - kA \left.\frac{d\Delta T(x)}{dx}\right|_{x=0.375\mu m}. \quad (3)$$

By substituting Eq. (2) into Eq. (3), the power absorbed by the CNT is solved for $\dot{Q} = (m_L + m_R)kA\Delta T_H$.[7] The ratio between the power absorbed and the incident laser power is equal to the optical absorption probability $\alpha = \dot{Q}/P_{laser}$, which ranges from 5.9×10^{-6} to 2.8×10^{-5} for this dataset. Table I shows the sample geometries and measurement results of three CNTs where electrical contacts were made to the CNTs.

The thermal conductivity of the ultra-long suspended CNT bundles measured in this work is found to be 1 to 2 orders of magnitude smaller than the values for single suspended CNTs reported in previous works, which range from 300 to 3400 W/m K.[25,26] However, it is hard to compare either the nanotube length or the diameter dependence of the thermal conductivity in these previous works with the CNTs reported in our work, because our measured samples include around 4 to 7 single CNTs instead of one single CNT. Here, we compare the thermal conductivity of CNT bundles measured with the values observed in our previous work on CNT bundles with similar diameters but shorter lengths (11 to 14 μm).[17] We find that the measured thermal conductivity of these CNT bundles is of the same order as those in our previous work. These results are also similar to those found on 10 nm and 148 nm diameter CNT bundles measured by Shi *et al.*[27] In addition, recent combined structure and thermal conductance measurements have indicated the strong effect of defect scattering on the thermal conductivity of CVD CNTs.[10] We then can conclude that the low measured thermal conductivities found in this work are due to defects and the strong coupling of phonons at the intertube contact.[28]

The heat transfer coefficients g determined from our measurements are based on the measured values of the thermal conductivity and span a range from 1.5×10^3 to 7.9×10^4 W/m^2 K. This is lower than the value calculated from classical gas kinetic theory, and it is also lower than the value simulated by Hu *et al.* (1×10^5 W/m^2 K). This discrepancy could have two origins. First, the accommodation coefficient, which describes the ratio of the actual energy exchange between the CNT and impinging air molecules to the ideal energy exchange, is most likely less than 1. In other words, an accommodation coefficient of 1 corresponds to the case in which the scattered gas molecules are in thermal

Downloaded 26 Sep 2011 to 128.125.121.154. Redistribution subject to AIP license or copyright; see http://jap.aip.org/about/rights_and_permissions

equilibrium with the CNTs. Second, the diffusive thermal resistance in the surrounding air can make the measured heat transfer coefficient lower than the thermal boundary conductance.

We find that the effective thermal conductivity of the sample during the laser heating measurement might differ from the thermal conductivity measured using the electrical heating method in vacuum if the average temperature of the CNT varies significantly. For sample 1 listed in Table I, the average temperature changes measured during electrical and optical heating are 473 K and 348 K, respectively. Although one study suggests that the thermal conductivity of a high-quality SWCNT sample is inversely proportional to the temperature above room temperature because of increased Umklapp scattering,[26] the measured thermal conductivities of CNTs grown via the CVD method exhibit rather weak temperature dependences between 300 and 500 K.[10] Moreover, the nearly linear temperature profile shown in Fig. 3(a) resembles the solution of the heat diffusion equation with a constant thermal conductivity along the nanotube. Nevertheless, the obtained k and g values from the measured temperature profiles are the average values between the 300 K cold side and the 500 to 650 K hot side temperatures. Furthermore, the Pd contacts used in this work should produce very low electrical contact resistances. Based on values of electrical contact resistance found in the literature,[29,30] we find that the electrical contact resistance has a negligible effect on our analysis. The variation in the electrical resistance among these three measured samples shown in Table I might result from differing numbers of semiconducting and metallic CNTs in the bundle or from defects in the samples. However, we cannot determine any real trends from this limited dataset of three nanotubes. Even though these nanotubes have relatively low thermal conductivities, the values of g and the decay lengths are valid.

III. CONCLUSION

In conclusion, we observe heat spreading along suspended CNTs and measure their heat transfer coefficient using a two-laser, non-contact, optical measurement technique. The heat exchange between single walled carbon nanotube (SWCNT) bundles and their surrounding air environment is found to be the dominant form of heat dissipation for nanotube bundles longer than 7 μm. When the SWCNT bundle is heated by a focused laser beam in vacuum, a constant temperature gradient is observed along the SWCNT at each side of the laser spot, consistent with diffusive transport. The absorbed power and the optical absorption probability of the CNTs are also determined from the measurement. In air, the exponentially decaying temperature profiles enable us to quantify the heat loss to air from the surface of the SWCNTs. The heat transfer coefficient, determined from these measurements, is found to lie between 1.5×10^3 and 7.9×10^4 W/m^2 K. These values are significantly higher than typical heat transfer coefficients between bulk materials and surrounding air environments because of the reduced diameter, making the SWCNT a good candidate for thermal management applications.

ACKNOWLEDGMENTS

This research was supported in part by DOE Award Nos. DE-FG02-07ER46376 and DE-FG02-07ER46377, and by NSF Award No. CBET-0854118.

[1]S. Berber, Y. K. Kwon, and D. Tomanek, Phys. Rev. Lett. **84**(20), 4613 (2000).
[2]P. B. Amama, C. Lan, B. A. Cola, X. Xu, R. G. Reifenberger, and T. S. Fisher, J. Phys. Chem. C **112**(49), 19727 (2008).
[3]B. A. Cola, J. Xu, and T. S. Fisher, Int. J. Heat Mass Transfer **52**(15–16), 3490 (2009).
[4]M. A. Panzer, G. Zhang, D. Mann, X. Hu, E. Pop, H. Dai, and K. E. Goodson, Trans. ASME Ser. C: J. Heat Transfer **130**(5), 052401 (2008).
[5]T. Tong, Y. Zhao, L. Delzeit, A. Kashani, M. Meyyappan, and A. Majumdar, IEEE Trans. Compon. Packag. Technol. **30**(1), 92 (2007).
[6]K. Kordas, G. Toth, P. Moilanen, M. Kumpumaki, J. Vahakangas, A. Uusimaki, R. Vajtai, and P. M. Ajayan, Appl. Phys. Lett. **90**, 123105 (2007).
[7]D. P. Dewitt, F. P. Incropera, T. L. Bergman, and A. S. Lavine, *Fundamentals of Heat and Mass Transfer*, 6th ed. (Wiley, New York, 2007).
[8]P. Kim, L. Shi, A. Majumdar, and P. L. McEuen, Phys. Rev. Lett. **8721**(21), 215502 (2001).
[9]C. H. Yu, L. Shi, Z. Yao, D. Y. Li, and A. Majumdar, Nano Lett. **5**(9), 1842 (2005).
[10]M. T. Pettes and L. Shi, Adv. Funct. Mater. **19**(24), 3918 (2009).
[11]H. Y. Chiu, V. V. Deshpande, H. W. C. Postma, C. N. Lau, C. Miko, L. Forro, and M. Bockrath, Phys. Rev. Lett. **95**(22), 226101 (2005).
[12]W. Yi, L. Lu, D. L. Zhang, Z. W. Pan, and S. S. Xie, Phys. Rev. B **59**(14), R9015 (1999).
[13]T. Y. Choi, D. Poulikakos, J. Tharian, and U. Sennhauser, Nano Lett. **6**(8), 1589 (2006).
[14]V. V. Deshpande, S. Hsieh, A. W. Bushmaker, M. Bockrath, and S. B. Cronin, Phys. Rev. Lett. **102**(10), 105501 (2009).
[15]Q. W. Li, C. H. Liu, X. S. Wang, and S. S. Fan, Nanotechnology **20**(14), 145702 (2009).
[16]I. K. Hsu, R. Kumar, A. Bushmaker, S. B. Cronin, M. T. Pettes, L. Shi, T. Brintlinger, M. S. Fuhrer, and J. Cumings, Appl. Phys. Lett. **92**(6), 063119 (2008).
[17]I. K. Hsu, M. T. Pettes, A. Bushmaker, M. Aykol, L. Shi, and S. B. Cronin, Nano Lett. **9**(2), 590 (2009).
[18]I. K. Hsu, M. T. Pettes, M. Aykol, L. Shi, and S. B. Cronin, J. Appl. Phys. **108**(8), 084307 (2010).
[19]C. F. Carlborg, J. Shiomi, and S. Maruyama, Phys. Rev. B **78**(20), 8 (2008).
[20]S. Shenogin, L. P. Xue, R. Ozisik, P. Keblinski, and D. G. Cahill, J. Appl. Phys. **95**(12), 8136 (2004).
[21]M. Hu, S. Shenogin, P. Keblinski, and N. Raravikar, Appl. Phys. Lett. **90**(23), 231905 (2007).
[22]J. Jeans, *An Introduction of the Kinectic Theory of Gases* (Cambridge University Press, New York, 1967).
[23]T. H. Brintlinger, PhD Thesis, University of Maryland, p. 139, 2005.
[24]F. M. Huang, K. T. Yue, P. H. Tan, S. L. Zhang, Z. J. Shi, X. H. Zhou, and Z. N. Gu, J. Appl. Phys. **84**(7), 4022 (1998).
[25]T. Y. Choi, D. Poulikakos, J. Tharian, and U. Sennhauser, Appl. Phys. Lett. **87**, 013108 (2005).
[26]E. Pop, D. Mann, Q. Wang, K. Goodson, and H. J. Dai, Nano Lett. **6**(1), 96 (2006).
[27]L. Shi, D. Y. Li, C. H. Yu, W. Y. Jang, D. Kim, Z. Yao, P. Kim, and A. Majumdar, Trans. ASME Ser. C: J. Heat Transfer **125**(5), 881 (2003).
[28]D. J. Yang, S. G. Wang, Q. Zhang, P. J. Sellin, and G. Chen, Phys. Lett. A **329**(3), 207 (2004).
[29]A. Javey, J. Guo, Q. Wang, M. Lundstrom, and H. J. Dai, Nature **424**(6949), 654 (2003).
[30]Z. H. Chen, J. Appenzeller, J. Knoch, Y. M. Lin, and P. Avouris, Nano Lett. **5**(7), 1497 (2005).

Downloaded 26 Sep 2011 to 128.125.121.154. Redistribution subject to AIP license or copyright; see http://jap.aip.org/about/rights_and_permissions